Heliyon 9 (2023) e21381

Contents lists available at ScienceDirect

Heliyon

journal homepage: www.cell.com/heliyon

Identification and validation of a novel signature based on T cell marker genes to predict prognosis, immunotherapy response and chemotherapy sensitivity in head and neck squamous carcinoma by integrated analysis of single-cell and bulk RNA-sequencing

Chongchang Zhou [a,1], Hongxia Deng [a,1], Yi Fang [a,b], Zhengyu Wei [a,b], Yiming Shen [a,b], Shijie Qiu [a], Dong Ye [a], Zhisen Shen [a,*], Yi Shen [a,c,**]

[a] Department of Otorhinolaryngology Head and Neck Surgery, Ningbo Medical Center Lihuili Hospital, Ningbo University, Ningbo, Zhejiang, China
[b] Health Science Center, Ningbo University, Ningbo, Zhejiang, China
[c] Department of Otorhinolaryngology Head and Neck Surgery, Ningbo NO. 2 Hospital, Ningbo, Zhejiang, China

ARTICLE INFO

Keywords:
Head and neck squamous carcinomas
T cell
Prognosis
Immunotherapy
Chemotherapy

ABSTRACT

T cells are among the most potent anti-tumor cells that are found in humans. Our study sought to develop a reliable signature incorporating T cell marker genes (TMGs) for predicting the prognosis and therapy responsiveness of head and neck squamous cell carcinoma (HNSCC) patients. We downloaded scRNA-seq data from the GSE181919 to identify TMGs. Subsequently, we devised a 12 TMG signature in the TCGA HNSCC cohort by using LASSO analysis. Patients with high-risk scores were shown to experience unfavorable progression-free survival, disease-specific survival, and overall survival, which was validated in the GSE65858 cohort. Additionally, the nomogram integrated risk score and clinical features are more suitable for clinical application. The enrichment analyses of both pathways and functions showed that high- and low-risk patients had functionally related distinctions. Furthermore, analysis of the immunological landscape confirmed that the low-risk patients had a larger percentage of infiltrating immune cells as well as a higher incidence rate of immune-related events. In the meantime, a greater IPS score and expression of immune checkpoint genes suggested significantly favorable responsiveness to immunotherapy in low-risk patients. On the other hand, the high-risk patients had a greater degree of sensitivity to the chemotherapy agents, which included paclitaxel, gemcitabine, docetaxel, and cisplatin. Our finding revealed that this TMG signature independently functioned as a prognostic marker and guided individualized immunotherapy and chemotherapy selection for patients with HNSCC.

* Corresponding author. Department of Otorhinolaryngology Head and Neck Surgery, Ningbo Medical Center Lihuili Hospital, Ningbo, 315040, Zhejiang, China.
** Corresponding author. Department of Otorhinolaryngology Head and Neck Surgery, Ningbo NO. 2 Hospital, Ningbo, 315099, Zhejiang, China.
E-mail addresses: szs7216@163.com (Z. Shen), tyzdhs@163.com (Y. Shen).
[1] These authors contributed equally to this work.

https://doi.org/10.1016/j.heliyon.2023.e21381
Received 3 April 2023; Received in revised form 15 September 2023; Accepted 20 October 2023
Available online 21 October 2023

1. Introduction

Head and neck cancer serves as the sixth most commonly encountered form of malignancy in the world [1], among which head and neck cancer squamous carcinoma (HNSCC) represents the main histological subtype for over 90 % of all head and neck cancers [2]. HNSCC arises from the mucosal epithelium of the upper respiratory and digestive tracts and it is associated with the prevalence of human papillomavirus infections, alcohol consumption, betel quid intakes, and tobacco use [3]. The global annual incidence of HNSCC comprises more than 870,000 cases, resulting in more than 440,000 deaths every year [4]. HNSCC patients are commonly diagnosed with advanced diseases and have a high probability of recurrence, leading to a correspondingly poor prognosis [5]. Notwithstanding the recent significant progress in comprehensive and multidisciplinary therapeutic approaches, includingsurgical resection, chemotherapy, radiotherapy, immunotherapy, and targeted therapy [6,7], aconsiderable improvement in 5-year survival has not occurred, and it is still lower than 50 % [8]. Diagnoses at an early stage and prognosis predictions are beneficial for advancing precision medicine and improving patient outcomes [9,10]. Nonetheless, conventional risk classification indicators based only on histological grades, distant metastasis, lymph node, and tumor size have a limited capacity in properly forecasting prognosis within individuals with HNSCC [11,12]. Consequently, developing novel and reliable prognostic signatures for patients with HNSCC is an urgent need.

T cells are a heterogeneous subset of cells that are extremely essential and perform critical functions in the adaptive immune system [13]. After T cell receptors (TCR) recognize the specific antigens, naive T cells could be differentiated into distinct effector T cells for participation in a variety of immunologic functions. Some of the more prevalent and well-recognized subpopulations of T cells include $CD8^+$ T Cells (cytotoxic T cells or killer T cells), $CD4^+$ T cells (helper T cells), and regulatory T cells (Tregs), which perform

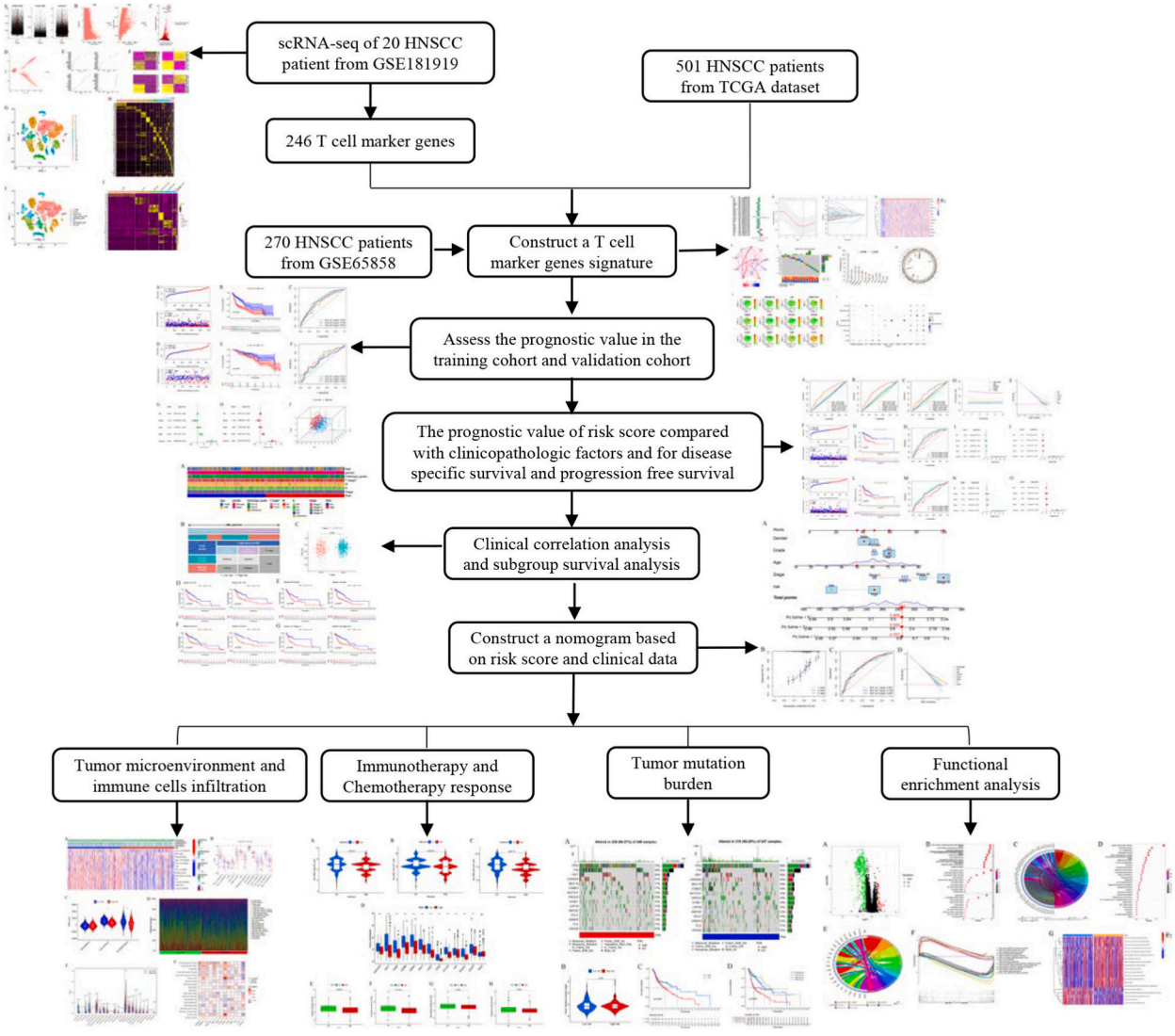

Fig. 1. The schematic flow diagram for this investigation.

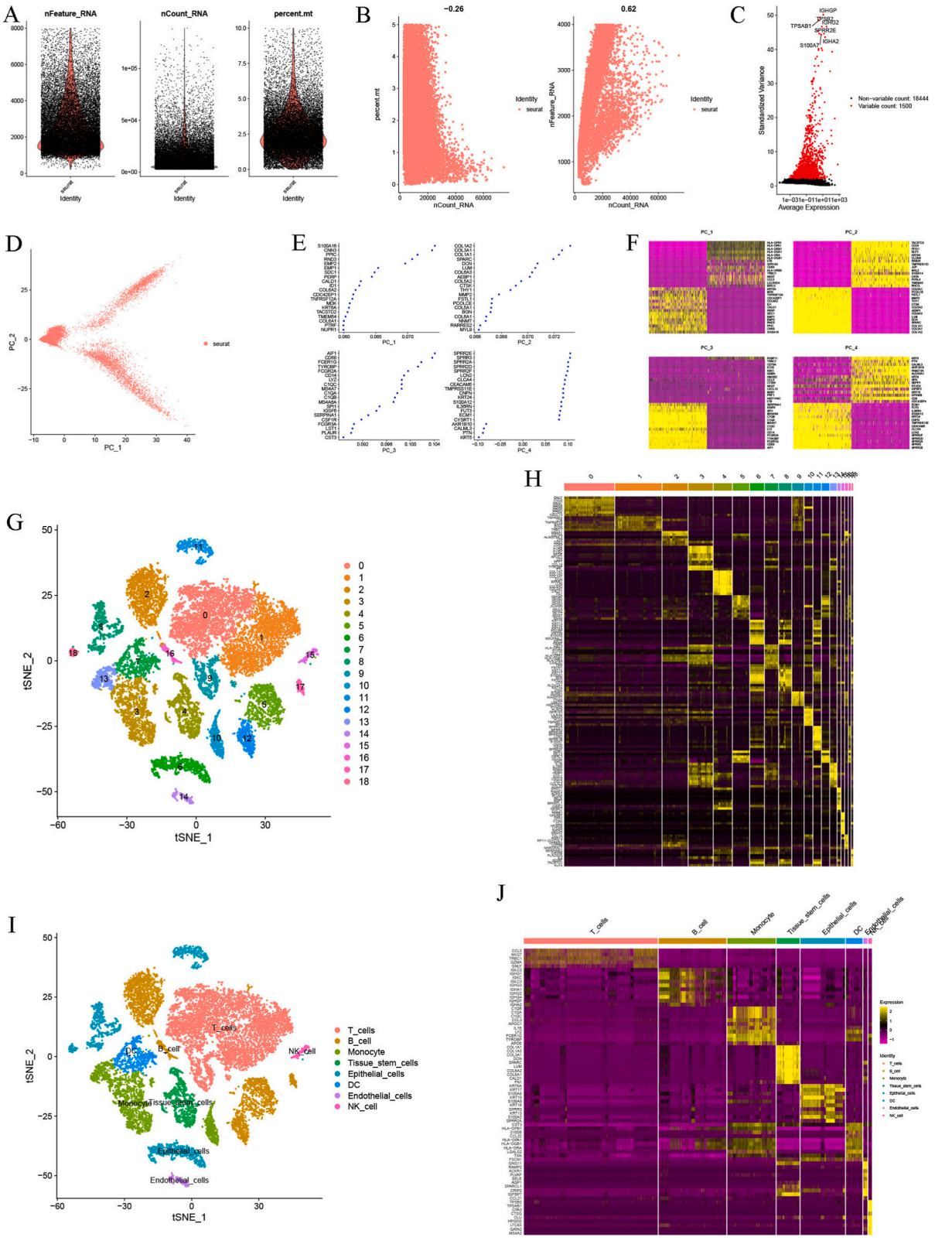

(caption on next page)

Fig. 2. scRNA-seq analysis revealed different clusters and cell types of HNSCC single-cell. A: The sequencing depth (shown on the left), the gene count (shown in the center), and the proportion of the mitochondrial genome (right) are shown using violin plots. B: The link between sequencing depth and the proportion of the mitochondrial genome and the total number of intracellular sequences was established using a dot plot. C: The correlation variance of the expression of each gene across all single-cell samples is displayed using dot plots. The top 1500 highly variable genes were denoted as red dots. D: Principal component analysis (PCA). E: Dot plot and F: Heatmap show the feature genes in the PCs. G: tSNE plot shows the regrouping of HNSCC single cells into 19 separate clusters. H: The 10 leading marker genes for each cluster are presented via a heatmap. I: tSNE plot shows the regrouping of HNSCC single cells into 8 cell types. J: The top 10 marker genes for each cell type are presented using a heatmap.

fundamental functions in the tumor microenvironment (TME) [14]. Cancer or stromal cells inside the TME release several immunosuppressive molecules such as interleukin 6 (IL-6), IL-10, and prostaglandin E2 to achieve immune tolerance and immunosurveillance evasion by regulating T cell activations [15]. Inanimate T cells are called exhausted T cells characterized by the expression of inhibitory molecules, which inhibit normal T-cell activations, thereby inhibiting anti-tumor immune function and promoting the tumor's growth [16]. Therefore, blocking the immune checkpoints inhibitors (ICIs) of T cells, including anti-cytotoxic T-lymphocyte-associated protein 4 (CTLA-4) and anti-programmed cell death protein 1/programmed cell death protein ligand 1 (PD-1/PD-L1), attracted substantial attention in cancer treatments, including HNSCC [17,18]. Additionally, multiple subtypes of T cells are linked to the prognosis of HNSCC [19–21]. Nevertheless, the exact processes of T cell marker genes (TMGs) in the TME and their involvement in patient prognosis and immunotherapy responsiveness in HNSCC are incompletely understood.

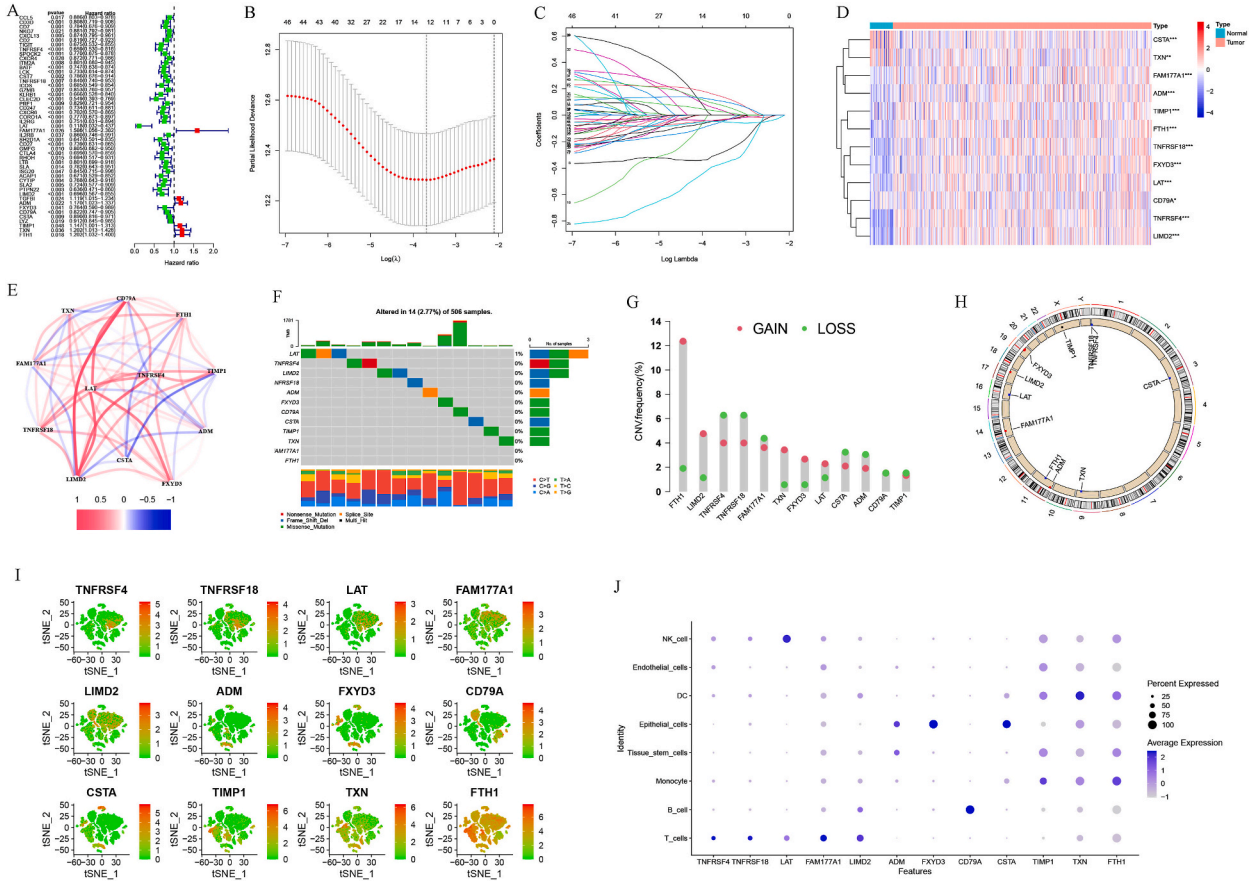

Fig. 3. Construction of T cell marker gene signatures correlated with overall survival in patients with HNSCC. A: Forest plot demonstrated different expressed T cell marker genes (TMGs) with considerable prognostic value in the TCGA-HNSC cohort. B: Profiles of the TMGs in the signature derived using the least absolute shrinkage and selection operator (LASSO). C: A visualization of the partial likelihood deviation vs. the log scale (lambda). The lambda value that results in the least amount of error is denoted by the vertical dotted line, which also denotes the highest possible value of lambda for which the deviation is within one standard error of the minimum. D: A heatmap was used to visually contrast the levels of the expression of the twelve TMGs that made up the signature in the HNSCC and normal samples. E: Interaction network of twelve TMGs. F: A landscape depicting the mutational characteristics of twelve TMGs found in individuals with HNSCC. G: CNV frequency of 12 TMGs. H: Chromosomal location of the CNV alternation of 12 TMGs. The red dots indicate an increase in the CNV gains of a sample in contrast with CNV losses, whereas the blue dots denote an increase in CNV losses in contrast with CNV gains. The presence of the black dot indicates that both are equivalent. I and J: The tSNE method was used to classify distinct cell types, and the expression level of each of the twelve TMG signature genes was compared across all of these cell types.

Single-cell RNA sequencing (scRNA-seq) is a promising approach for evaluating the transcriptomes at a single-cell level. scRNA-seq has the potential to uncover extensive intertumoral heterogeneity in contrast with the traditional method of determining the average gene expression in all cells [22]. Furthermore, the scRNA-seq analysis facilitates researchers in identifying crucial genes that are specific to certain cell types [23]. Moreover, several researchers have used scRNA-seq analysis to construct efficient prognostic models in the numerous cancers [24,25]. Herein, we firstly gathered the scRNA-seq data of HNSCC from the Gene Expression Omnibus (GEO) database to distinguish T cell subclusters and identify TMGs. We aimed to construct the TMG signature linked to the HNSCC prognosis using the least absolute shrinkage and selection operator (LASSO) analysis in the Cancer Genome Atlas (TCGA)-HNSCC cohort and validate in the GSE65858 dataset. We also examined the association of the TMG signature with TME, immune cell infiltration, responsiveness to immunotherapy, and susceptibility to chemotherapy. Our analysis indicates that this TMG signature might serve as an independent prognostic indicator and offer novel guidance for the customized selection of immunotherapy and chemotherapy in HNSCC.

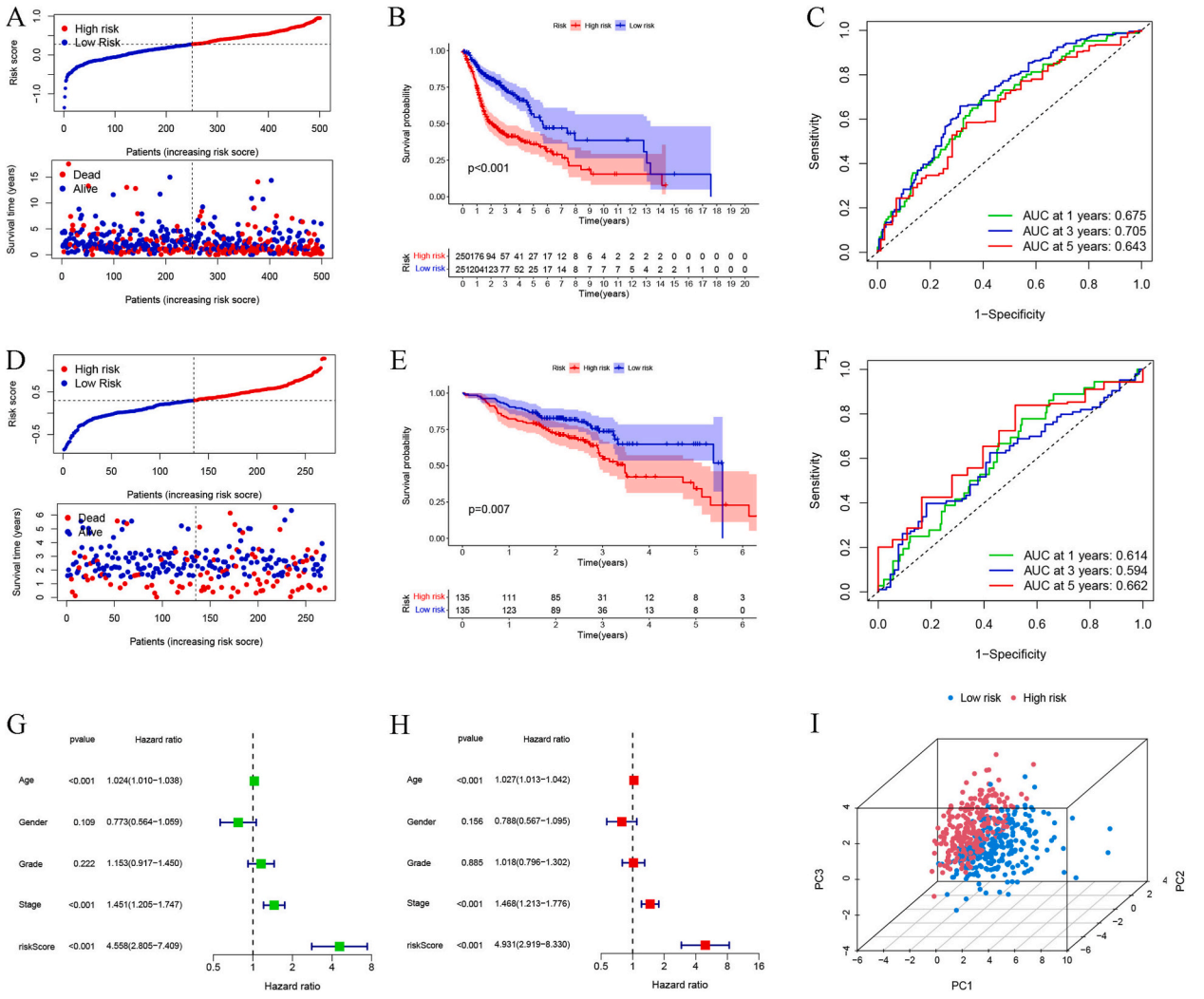

Fig. 4. Verification of the TMG signature's predictive value. A: Risk score, survival time, and survival rate distribution in the TCGA cohort. B: The Kaplan–Meier estimate of survival time for the TCGA dataset based on the TMG signature. C: Survival rates over 1, 3, and 5 years for the TCGA dataset as judged by the ROC curve of the TMG signature. D: The risk score, survival time, and status distribution in the validation cohort. E: TMG signature-based Kaplan–Meier survival analysis in the validation set. F: The TMG signature's ROC curve for 1-, 3-, and 5-year survival in the validation set. Univariate (G) and multivariate (H) Cox regression analysis of the TMG signature in the TCGA cohort. I: The principal component analysis of the TMG signature.

2. Results

2.1. scRNA-seq analysis identified T cell mark genes of HNSCC

Fig. 1 depicts all of the processes involved in processing and analyzing the data. Firstly, we executed the quality control and normalization (Fig. 2A, B, and C) operations of the scRNA-Seq from GSE181919, including 20 HNSCC samples. Secondly, via PCA (Fig. 2D, E, and F) and t-SNE dimensionality reductions, we identified 19 distinct clusters (Fig. 2G). Fig. 2H displays the ten leading marker genes for each cluster. Thirdly, the 19 clusters were annotated and re-grouped into 8 cell types (Fig. 2I) based on the "SingleR" package. Among the 19 clusters, clusters 0, 1, and 9 were identified as T cell subtypes. Finally, with the help of FindAllMarkers, we screened the differentially expressed marker genes across the 8 selected cell types. Fig. 2J depicts the ten leading marker genes for each cell subset. In total, 246 TMGs were identified for subsequent analyses.

2.2. Development of the T cell marker genes signature

As illustrated in Figs. 3A and 49 differentially expressed prognostic TMGs with differential expression were discovered via differential and univariate Cox survival analyses and subsequently subjected to LASSO analysis to eliminate overfitting signatures (Fig. 3B and C). In the end, 12 TMGs were used to develop the signature. Each sample was assigned a risk score using the following formula: risk score = (−0.301) × *TNFRSF4* expression+(−0.037) × *TNFRSF18* expression+(−0.381) × *LAT* expression+(0.052) × *FAM177A1* expression+(−0.044) × *LIMD2* expression+(0.032) × *ADM* expression+(−0.064) × *FXYD3* expression+(−0.047) × *CD79A* expression+(−0.039) × *CSTA* expression+(0.154) × *TIMP1* expression+(0.087) × *TXN* expression+(0.114) × *FTH1* expression. We separated the HNSCC samples of the TCGA and GSE65858 cohorts into low- and high-risk categories as per the median risk score. Moreover, we analyzed the landscape of 12 TMGs in HNSCC. The heatmap (Fig. 3D) showed the expression profiles of 12 TMGs. Notably, two of the TMGs were downregulated in tumor samples, including *CSTA* and *TXN5*, and the rest were all upregulated. As shown in Fig. 3E, the correlation of the 12 TMGs was investigated. The somatic mutation profile of the 12 TMGs was also summarized and showed extremely low mutation frequencies in the HNSCC (Fig. 3F). Fig. 3G and H shows the frequency of the CNV alterations of the 12 TMGs and their locations on the chromosome. For the 10 genes studied, CNVs were prevalent, with LOSS occurring more often than GAIN. The *FTH1* and *LIMD2* genes experienced the greatest CNV gains, whereas the *TNFRSF4* and *TNFRSF18* genes experienced the greatest CNV losses. The tSNE algorithm then determined that the expression of the 12 TMGs was differently expressed in the T cell cluster compared with the other cell clusters (Fig. 3I and J).

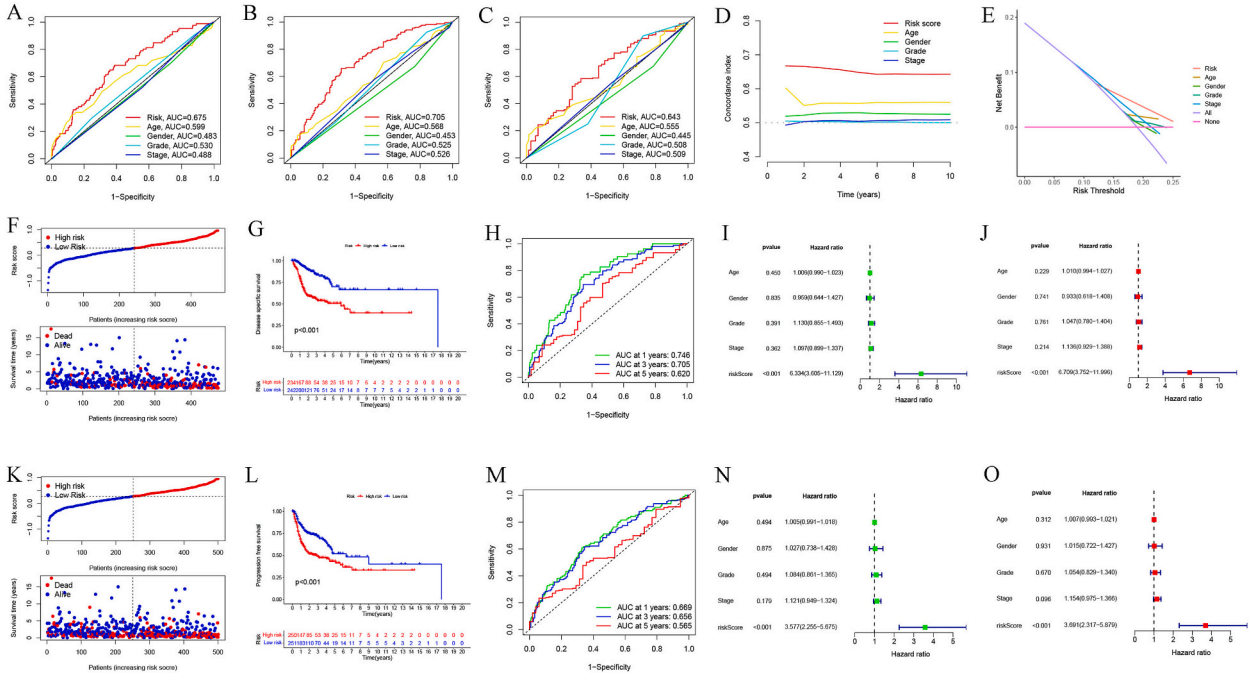

Fig. 5. ROC curves for predicting survival for 1-year (A), 3-year (B), and 5-year (C) periods based on risk score and clinical parameters. D: A time-related assessment evaluating the concordance between the risk score and clinical features E: A decision curve analysis (DCA) was performed using the risk score and clinical features. F: The risk score, survival status, and disease-specific survival (DSS) time distributions. G: Analysis of DSS using a Kaplan–Meier plot on the basis of the TMG signature. H: ROC curve of 1-, 3- and 5-year DSS. Univariate (I) and multivariate (J) Cox regression analysis of the risk score for DSS. K: The risk score, survival status, and progression-free survival (PFS) distributions. L: TMG-based Kaplan–Meier curve of PFS. M: ROC curve of 1-, 3- and 5- for PFS. Univariate (N) and multivariate (O) Cox regression analysis of the risk score for PFS.

2.3. Verification of the TMG signature

As illustrated in Fig. 4A, a greater risk score was linked to both lower survival times and increased death rates in the TCGA dataset. As per the findings of KM survival analysis, high-risk HNSCC patients exhibited a dismal OS relative to those in the low-risk category (Fig. 4B). We generated ROC curves for 1-, 3-, and 5-year OS to evaluate the effectiveness of the TMG signature, and their respective AUCs were 0.675, 0.705, and 0.643 (Fig. 4C). Our findings in the GSE65858 dataset were comparable with those in the TCGA dataset. As patients' risk scores increased, their fatality rates increased as well (Fig. 4D). Survival data from the GSE65858 dataset showed that low-risk patients fared better than those belonging to the high-risk group, as demonstrated by the Kaplan–Meier analysis ((Fig. 4E, P = 0.007). The GSE65858 dataset's AUCs for 1-, 3-, and 5-year OS were 0.614, 0.594, and 0.662, respectively (Fig. 4F). The risk score was proven to serve as a prognostic indicator in an independent manner for the OS of HNSCC patients, as shown by the findings of both

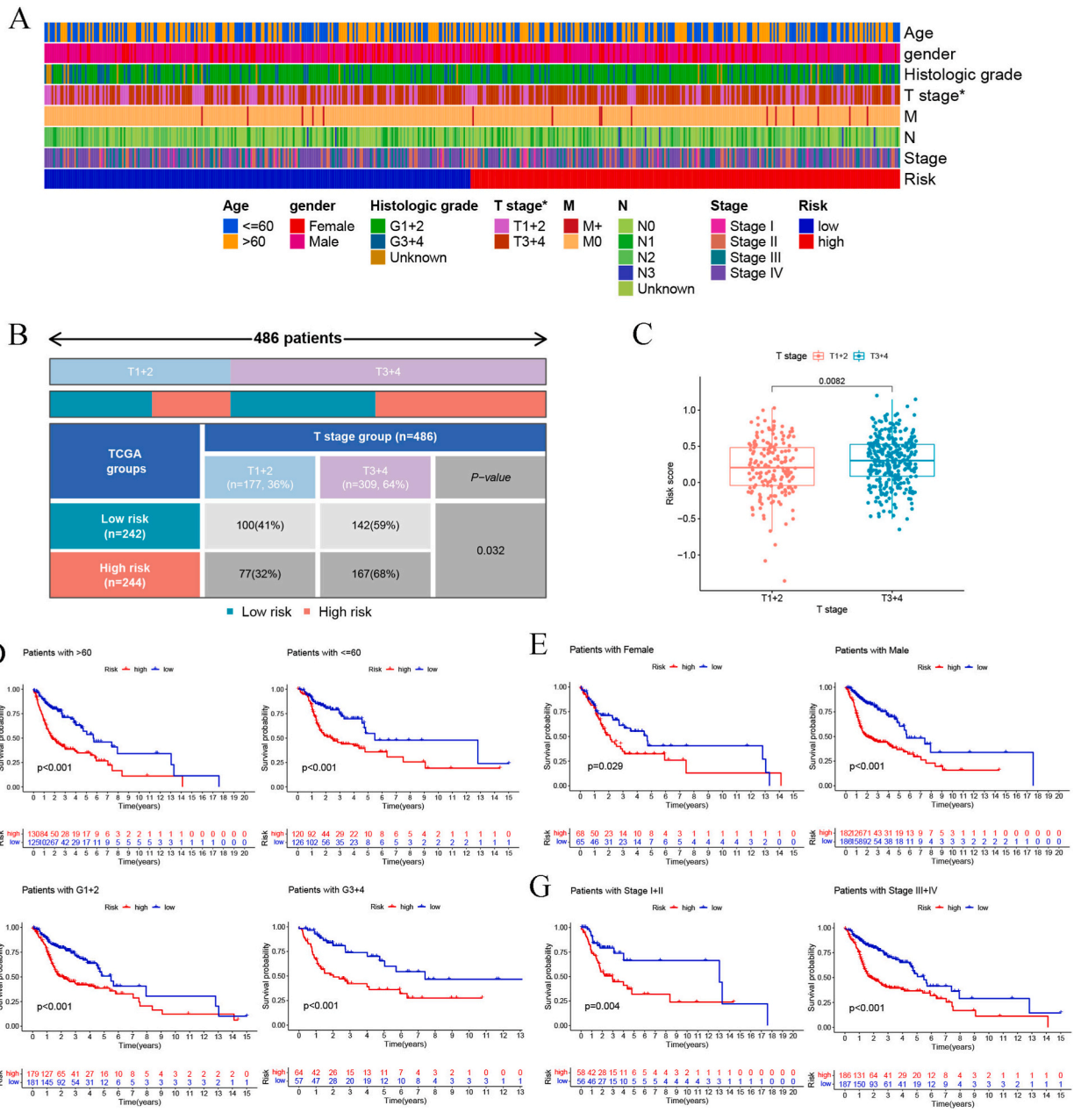

Fig. 6. Analysis of the correlations between the TMG signature and clinical characteristics and subgroup survival analysis. A: Comparative analysis of the high- and low-risk patients' clinical parameters is shown via a heatmap. B: The proportion of early and advanced T stage patients distributed across the two groups C: The difference in risk score between early and advanced T stage is demonstrated using box plots. The subgroup survival analysis based on age (D), gender (E), histologic grade (F), and clinical stage (G).

univariate (Fig. 4G) and multivariate (Fig. 4H) Cox regressions. The TMG signature was shown to differentiate between low- and high-risk patients using PCA (Fig. 4I). The time-dependent ROC for OS at 1 (Fig. 5A), 3 (Fig. 5B), and 5 (Fig. 5C) years showed that the risk score exhibited superior predictive performances in contrast with clinicopathological features. Furthermore, the concordance index (Fig. 5D) and DCA (Fig. 5E) concluded the same result. Then, we analyzed the prediction significance of the TME signature for DSS and PFS. Fig. 5F depicts each sample's risk score and DSS status distributions. High-risk HNSCC patients exhibited worse DSS than those in the low-risk category (Fig. 5G). When comparing 1-, 3-, and 5-year DSS, the AUC values were 0.746, 0.705, and 0.620, respectively, as shown by a time-dependent ROC analysis (Fig. 5H). Univariate (Fig. 5I) and multivariate (Fig. 5J) analyses confirmed that the risk score independently served as a reliable predictor of poor DSS. Fig. 5K displays the risk score and PFS status distributions for all samples. PFS was remarkably lowered in high-risk patients relative to the case among those in the low-risk category (Fig. 5L). One-, three-, and five-year PFS-AUC values of the ROC curve were 0.669, 0.656, and 0.565, respectively (Fig. 5M). Univariate (Fig. 5N) and multivariate (Fig. 5O) Cox models both disclosed that risk score served as a predictive marker for PFS in an independent manner.

2.4. Association of risk score with clinicopathological features

We used heatmaps to additionally examine and visualize the link between the risk score and clinical factors (Fig. 6A). Fig. 6B demonstrated that high-risk patients had a higher incidence of advanced T-stage cases than the low-risk category. However, we discovered that the risk score was greater in patients at the later T stage relative to those at the earlier stage (Fig. 6C). Additionally, the subgroup's survival analysis based on clinical parameters (age: Fig. 6D; gender: Fig. 6E; histologic grade: Fig. 6F; clinical stage: Fig. 6G) demonstrated that, in all subgroups, individuals at higher risk had a worse OS than those at lower risks.

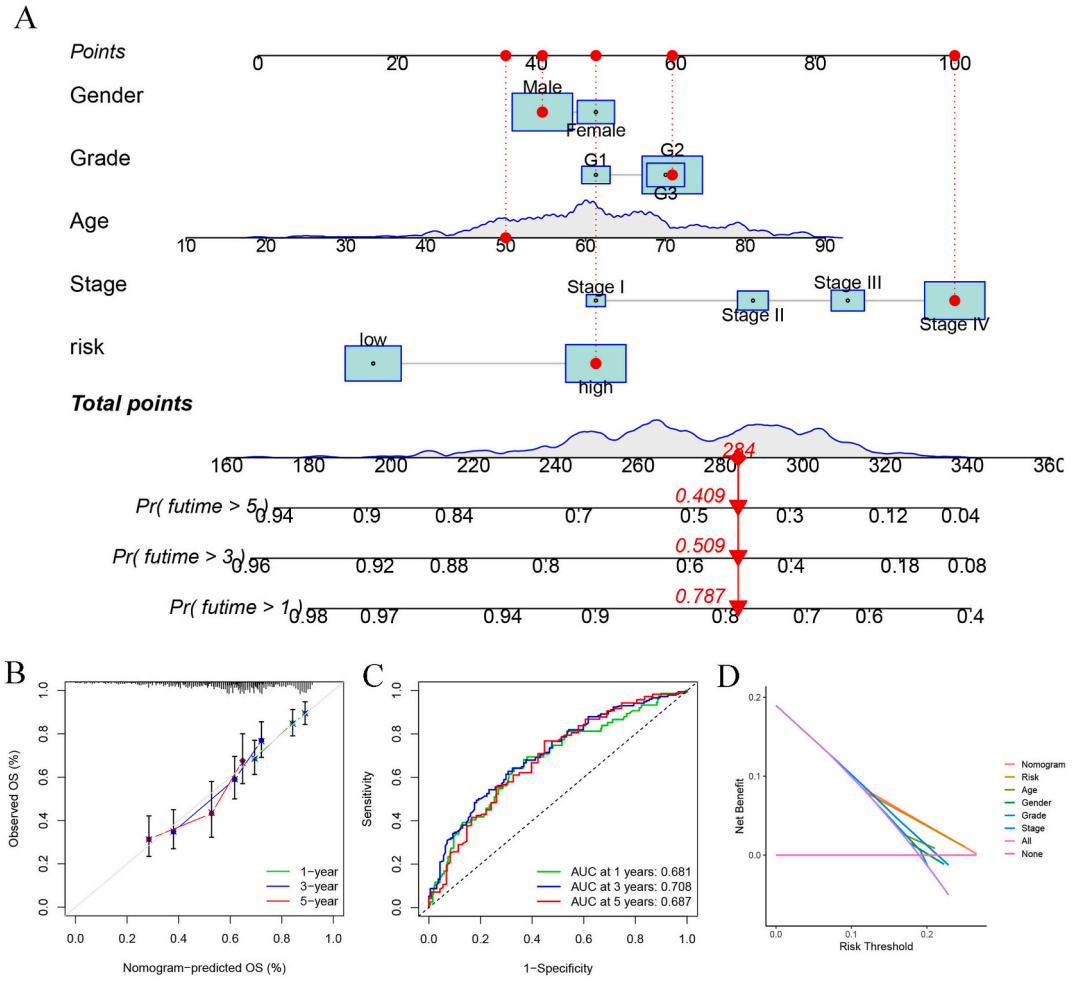

Fig. 7. Nomogram for predicting patients' prognoses in HNSCC. A: A nomogram was developed by integrating the risk score with the clinical and pathological characteristics in the TCGA dataset. B: The calibration curves of the nomogram used to anticipate OS over 1, 3, and 5 years. C: ROC curves for one-, three-, and five-year survival based on the nomogram's predictions. D: DCA plots were created for comparisons between the risk score and the clinical and pathological variables.

2.5. Nomogram formulation and verification

The risk score and clinical data were employed to develop a nomogram for anticipating OS in the TCGA dataset, which could additionally enhance the clinical value of the risk signature (Fig. 7A). Good consistency between predicted and actual values was shown in the calibration curves for 1-, 3-, and 5-year OS, demonstrating that the nomogram anticipated the OS of HNSCC patients in an accurate manner (Fig. 7B). One-, three-, and five-year ROC curves had AUCs of 0.681, 0.706, and 0.687, respectively (Fig. 7C), which showed the better predictive power of the risk score compared to the clinical characteristics. For the prognosis prediction of HNSCC patients, the nomogram outperformed both dependent clinical parameters and risk score, as demonstrated by the DCA curve (Fig. 7D).

2.6. Functional enrichment analysis

We delved deeper to discover how high- and low-risk patients varied in terms of biological processes and signaling pathways. Therefore, we used 519 DEGs (Fig. 8A) across the two risk categories to conduct a GO and KEGG enrichment analysis. The DEGs were shown to have an enrichment of biological functions related to the immune system, as shown by the GO analysis (Fig. 8B and C). The KEGG analysis (Fig. 8D and E) indicated that the DEGs joined mainly in many immune-associated pathways, including primary immunodeficiency, T cell receptor signaling pathway, chemokine signaling pathway, Th17 cell differentiation, cell adhesion molecules, and cytokine–cytokine receptor interactions. Additionally, the GSEA (Fig. 8F) and GSVA (Fig. 8G) analysis showed the enrichment of stromal-associated pathways in high-risk samples, including focal adhesion, galactose metabolism, glycosaminoglycan biosynthesis–chondroitin sulfate, and ECM-receptor interactions, as well as the enrichment of many immune-associated pathways in the low-risk samples, including natural killer cell-mediated cytotoxicity, T cell and B cell receptor signaling pathways, Fc epsilon RI signaling pathways, and chemokine signaling pathways.

2.7. Correlations between the TMG signature and tumor microenvironment

The heatmap (Fig. 9A) indicated the relationship of the TMG signature with the TME and immune function. The vast majority of immune function scores were considerably elevated in the low-risk category in contrast with the high-risk category, as determined by ssGSEA (Fig. 9B). When comparing the TMEs of low- and high-risk categories using the ESTIMATE method, we discovered that the former had higher values with respect to immuneScore and ESTIMATE scores (Fig. 9C), representing larger amounts of immune cellular components in the TME. Scores for 22 different types of immune cells were computed using the CIBERSORT algorithm. Fig. 9D illustrates the distribution patterns of these immune cell scores between low- and high-risk samples. Fig. 9E shows that the low-risk category had a higher proportion of active memory $CD4^+$ T cells, follicular helper T cells, regulatory T cells, and $CD8^+$ T cells. Fig. 9F illustrated the association of immune cell infiltration with the expression of TMGs in the signature, as well as the risk score. The

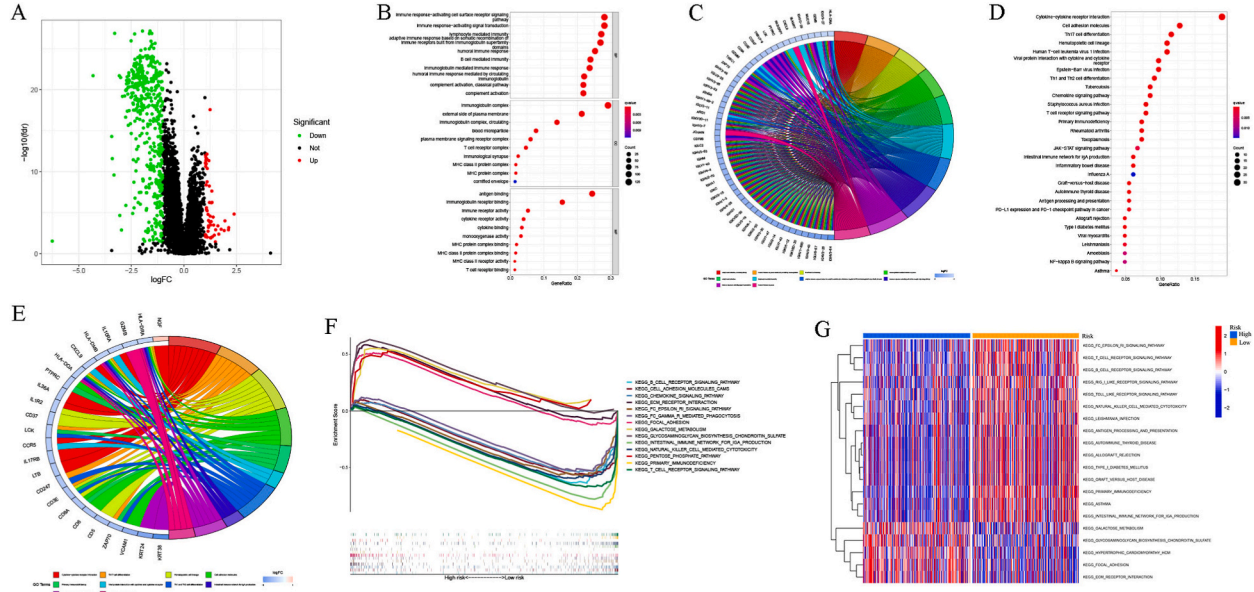

Fig. 8. Functional enrichment analysis between high- and low-risk patients. A: A volcano graphic depicting the differentially expressed genes (DEGs) between high- and low-risk categories. The color red indicates genes with increased expression, while blue indicates genes with decreased expression. The GO enrichment analysis based on DEGs, presented as a bubble chart (B) and chord plot (C). The KEGG pathway analysis based on DEGs presented as a bubble chart (D) and a chord plot (E). F: Gene set enrichment analysis (GSEA) between the two risk groups. G: Heatmap of gene set variant analysis (GSVA) between the two risk groups.

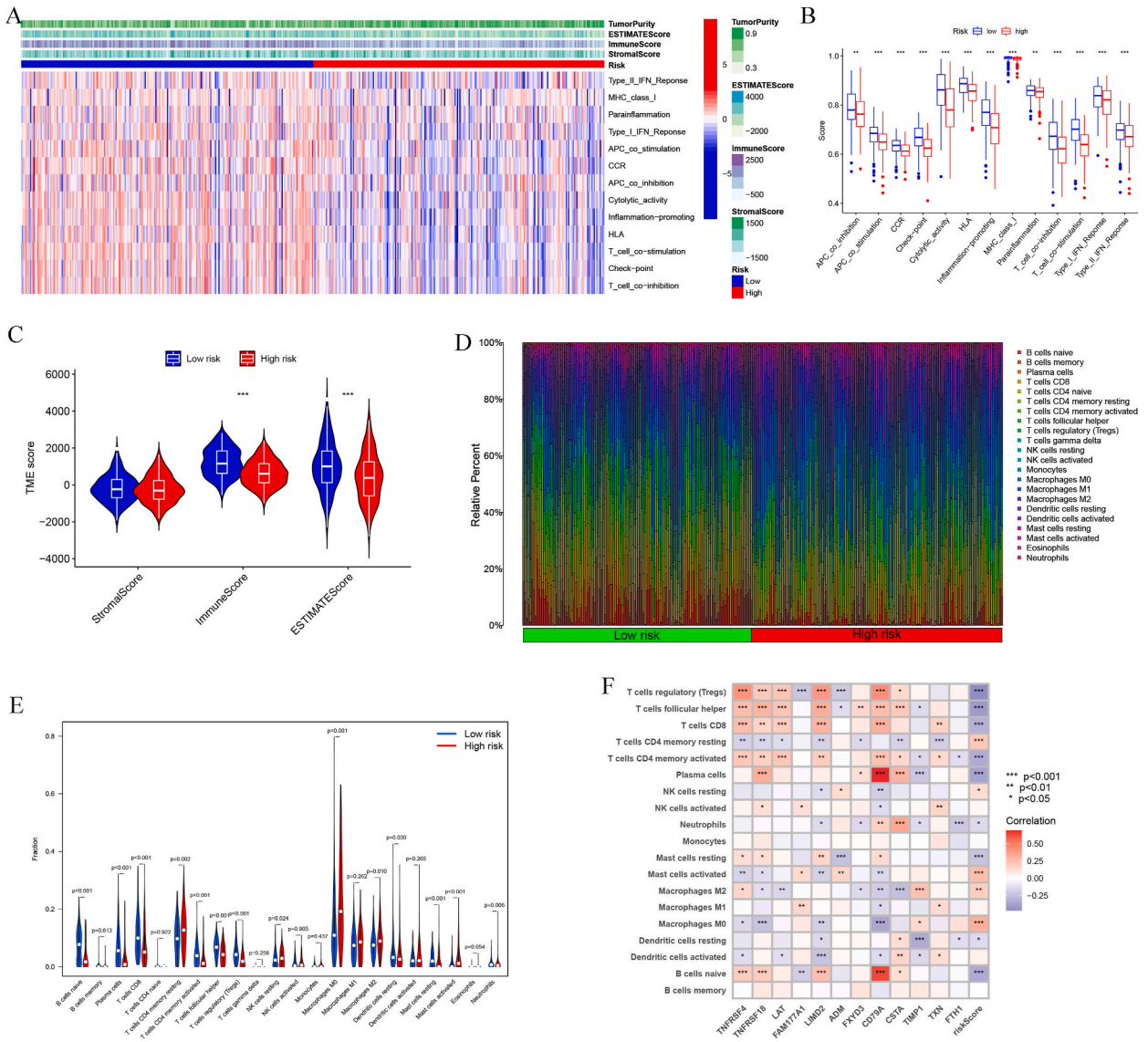

Fig. 9. The landscape of tumor microenvironment (TME) between high- and low-risk patients. A: The heatmap illustrates the differences in the tumor microenvironment and immune-associated functions between the two groups. B: The ssGSEA score of immune-related functions was compared across the two risk categories. C: Scores of stromal activity, immune activity, and the ESTIMATE score were compared between the two groups using the ESTIMATE method. D: The percentages of immune cell infiltration shown as bar plots for both the high- and the low-risk categories E: The proportions of immune cell infiltration were contrasted using a violin plot for high- and low-risk patients. F: The heatmap presented the relationship between immune cell infiltration, the expression of TMGs, and risk scores in a visual manner.

above findings demonstrated that low-risk patients exhibited an activated immune phenotype, which may partly help explain why those with a low-risk score for HNSCC tended to have a better prognosis.

2.8. Immunotherapy and chemotherapy response prediction

In terms of IPS, low-risk patients benefited more from PD1 blockade monotherapy (Fig. 10A), CTLA4 blockade monotherapy (Fig. 10B), and a combination of PD1 and CTLA4 blockade therapy (Fig. 10C) than high-risk patients. The low-risk patients had a greater likelihood of responding better to ICB treatments since their expressions of ICGs were remarkably enhanced (Fig. 10D). All of these findings corroborate that the TMG signature is useful for predicting whether or not immunotherapy would be effective in treating HNSCC. The sensitivity of four chemotherapy regimens for HNSCC was also assessed relative to the TMG signature by using the pRRophetic package. Increased sensitivity to a single medication is shown by a decrease in its IC50 value. As opposed to immunotherapy, high-risk patients with HNSCC may respond more sensitively to chemotherapy, including cisplatin (Fig. 10E), docetaxel

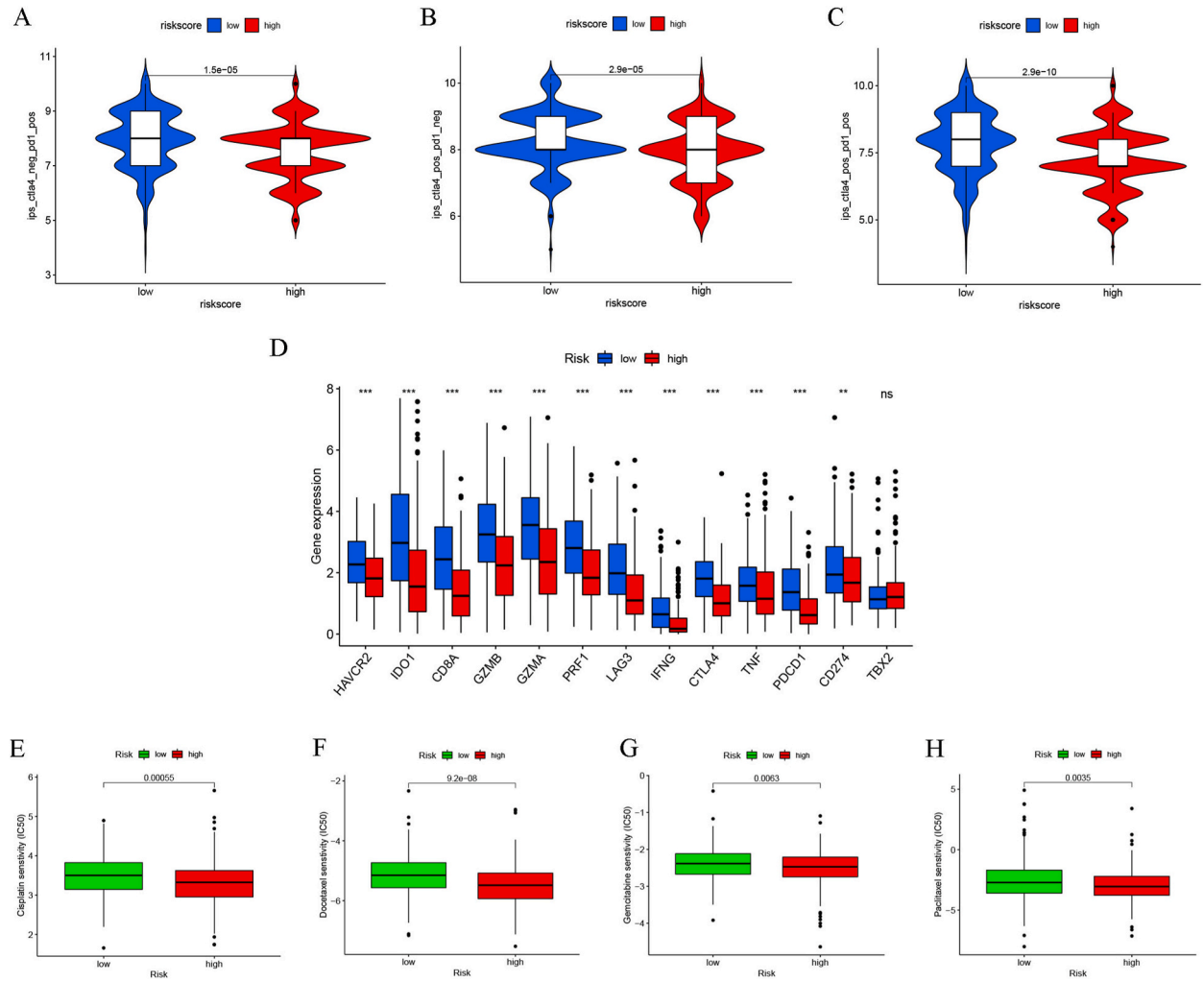

Fig. 10. Prediction of drug sensitivity and immunotherapy responsiveness. The IPS score of (A) PD1 blockade monotherapy; (B) and (C) combined PD1 and CTLA4 blockade therapy for high- and low-risk patients. D: Variations in immune checkpoint blockade gene expression between individuals at high and low risk. Variations in IC50 value of cisplatin (E), docetaxel (F), gemcitabine (G), and paclitaxel (H) across high- and low-risk patients.

(Fig. 10F), gemcitabine (Fig. 10G), and paclitaxel (Fig. 10H).

2.9. Gene mutation analysis associated with the TMG signature

As a first step, we separated patients into high- and low-risk score categories and displayed the genetic mutation distribution in each category. Somatic mutations were highly frequent in the high-risk patients relative to the low-risk category, as seen in the Waterfall plot (Fig. 11A) (96.37 vs. 88.26 %). Although no differential TMB between high- and low-risk samples was observed (Fig. 11B), the KM survival curve depicted a longer OS with low TMB levels compared with high TMB levels (Fig. 11C). As per the results of the survival study that combined both TMB and risk score, the low TMB and low-risk group had the best OS, while the high TMB and high-risk group had the worst outcomes (Fig. 11D).

3. Discussion

Given the insidious nature of the illness's early manifestations, a large proportion of HNSCC patients was confirmed with middle and advanced disease stages at the first diagnosis [26]. Despite the improvement of surgical, radiotherapy, and chemotherapy techniques, as well as the applications of personalized medicine, such as ICB and targeted medicines, the prognosis of HNSCC remains stubbornly poor [27]. Moreover, after undergoing therapy for HNSCC, the patient's quality of life dramatically declines, especially after mutilating surgeries [28]. Hence, it is crucial to investigate the processes behind HNSCC advancements and to discover novel

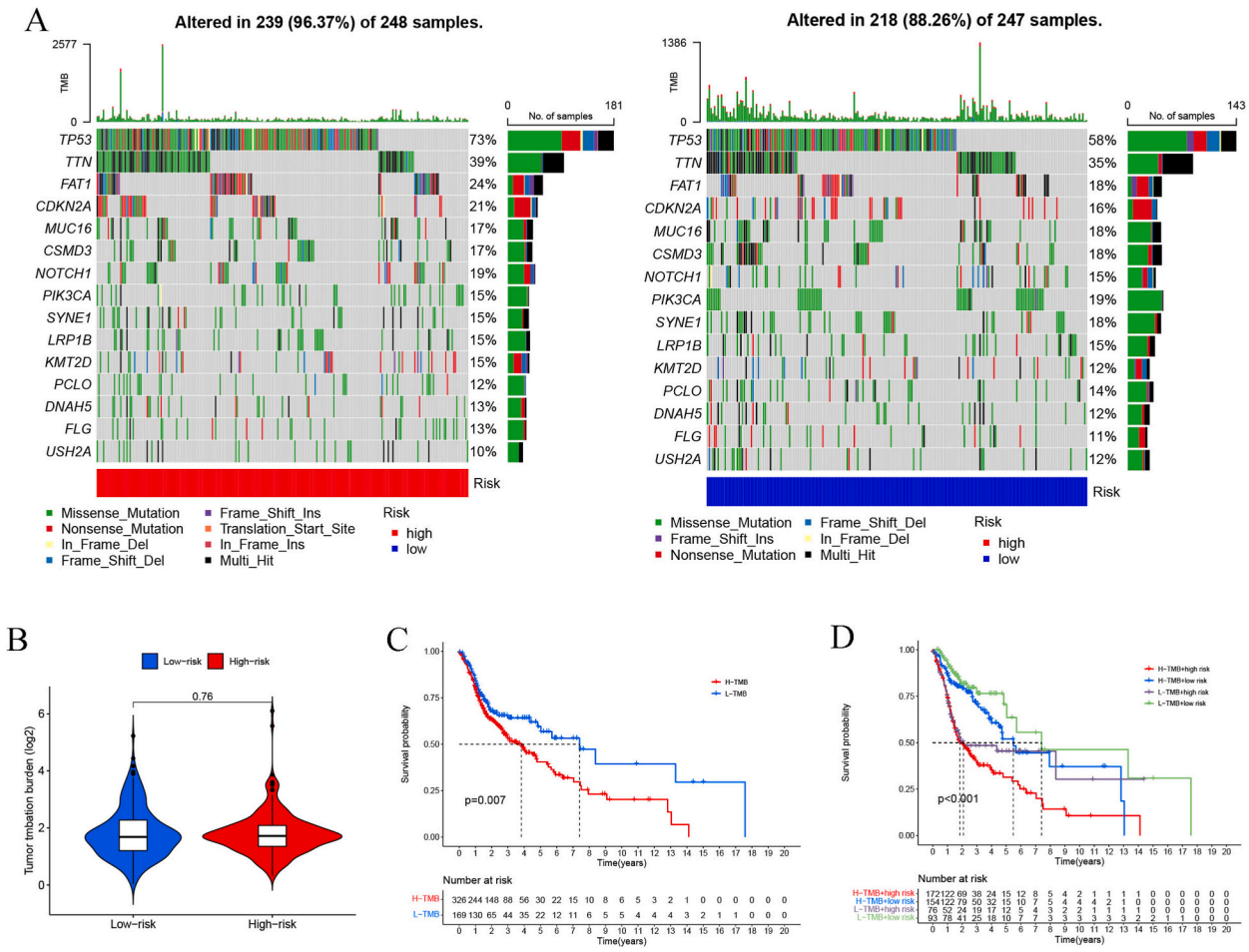

Fig. 11. The relationship between tumor mutation burden (TMB) and the TMG signature. A: The 15 most frequently mutated genes in the TCGA dataset across the low-risk and high-risk categories, as shown by a waterfall plot. B: Variations in TMB across high- and low-risk patients. C: Comparison of the high-TMB and low-TMB patients' survival curves. D: Survival curve combined TMB and risk score.

biological markers that might anticipate prognosis and therapy responsiveness in individuals with HNSCC.

The tumorigenesis and metastasis of HNSCC are remarkably influenced by the number and distribution of cells within the TME [29]. Among them, T cells are the most effective immune surveillance cells and assume indispensable functions in eliminating cancerous cells [30], and they could predict HNSCC patients' prognoses [31,32]. Additionally, T cell-related gene signature could be used for predicting prognosis and immune response in several cancers [33–35]. In this work, we first applied the scRNA-seq data of HNSCC patients to filter out T cell clusters and obtained 246 T cell marker genes. We developed a prognostic signature for HNSCC patients as per 12 TMGs using a LASSO regression analysis, including *TNFRSF4*, *TNFRSF18*, *LAT*, *FAM177A1*, *LIMD2*, *ADM*, *FXYD3*, *CD79A*, *CSTA*, *TIMP1*, *TXN*, and *FTH1*. *TNFRSF4* and *TNFRSF18* belong to the TNF-receptor superfamily and have been shown to participate in $CD4^+$ T cell responses and regulatory T cell-maintained dominant immunological self-tolerance, as well as in the proliferation and differentiation of B cells mediated by T cells [36,37]. Emerging evidence indicated that *TNFRSF4* is upregulated in several cancers and can serve as an unfavorable prognostic indicator [38–40]. *LAT* is crucial for the stimulation of the TCR signal transduction pathway and is linked to cancer chemotherapy and immunotherapy [41,42]. Liao et al. indicated that the overexpression of *FAM177A1* inhibited the transcription of inflammatory genes [43]. *LIMD2* may function as an oncogene in diverse cancers and is linked to dismal prognosis in esophageal cancer [44], clear cell renal cell carcinoma |(ccRCC) [45], ovarian cancer [46], and papillary thyroid carcinoma [47]. *FXYD3* acts as a member of the FXYD protein family correlated with Na+/K + -ATPase enzymes and serves critical biological functions in the advancement of multiple cancers and immunosuppressive TME [48,49]. Shiba et al. indicated that esophageal squamous cell carcinomas with CSTA overexpression in tumors were more likely to have progressed to a more advanced stage of the disease [50]. Conversely, Wang et al. proved that the lowered expression levels of CSTA increases lymphatic metastases and correlates with grim survival outcomes in oral squamous cell carcinoma [51]. *TIMP1* is a key element in the proteolytic degradation of the extracellular matrix and is extremely responsive to a wide variety of cytokines and hormones [52]. It is also associated with chemoresistance in pancreatic ductal adenocarcinoma [53]. *TXN* is considered a potent protein disulfide reductase involved in the regulation of cellular redox reactions [54]. Increased *TXN* expression may promote colon cancer cell migration and invasion [55],

and it is linked to dismal prognoses in ccRCC [56]. *FTH1* has a function in sustaining cellular iron homeostasis and participates in complicated pathways that may either enhance or prevent carcinogenesis [57]. However, no study reported the effect of *ADM* on T cells or its role in cancers. In the current work, we matched the expression patterns, somatic mutations, and CNVs of 12 TMGs and discovered that all of them exhibited differential expressions between tumor and normal samples. Although TMGs have a low mutation rate, most have had altered CNVs. This provides additional evidence that the aberrant expression of these TMGs may play an essential role in HNSCC.

Based on the 12 TMG signatures, we constructed the risk model and divided HNSCC patients into 2 different subgroups predicated on the median risk value. The KM curve for the OS illustrated that patients' prognoses could be differentiated by the risk model in the TCGA and GEO validation datasets. In line with the entire cohort, the risk model also can be applied to subgroup cohorts by clinical features. Importantly, univariate and multivariate analyses confirmed the risk score as a standalone prognostic indicator for poor outcomes in patients with HNSCC. Time-dependent ROC curves, time-related C-index curves, and decision curves were thereafter generated, and a detailed study indicated a more noticeable forecasting accuracy with respect to the risk score relative to other standard clinical factors such as age, clinical stage, histological grade, and sex. Furthermore, the prognostic efficacy for estimating the DSS and PFS of patients with HNSCC was also demonstrated by ROC curves, KM analysis, and Cox regression analysis. Taken together, the findings confirmed that the risk score was a reliable indicator for the risk classification and prognosis prediction of patients with HNSCC. Thus, for use in clinical settings, we combined the risk scores with clinical parameters to develop a nomogram. We found a strong consistency between the predicted and actual values using calibration curves, indicating that the nomogram could provide a precise survival rate prediction for HNSCC patients.

We conducted a GO analysis on the DEGs to investigate the possible mechanisms of the TMGs risk model in HNSCC and discovered the enrichment of these DEGs in biological functions related to the immune system. More specifically, our KEGG, GSEA, and GSVA analyses confirmed that cell adhesion and the synthesis of extracellular matrix (ECM) structure-related pathways were more active in high-risk patients and that this was associated with the initiation of tumor-cell invasion and metastasis [58,59]. In contrast, many immune pathways were primarily enriched in the low-risk category, including the T cell receptor signaling pathway, B cell receptor signaling pathway, and natural killer cell-mediated cytotoxicity, and all of them play a significant role in the transmission of immune signals and immune responses and in killing tumor cells [60,61], indicating that low-risk patients have higher immunogenicity.

As is well-known, immunotherapy offers new opportunities for cancer treatments in various tumor types, including HNSCC [17, 62]. Recently, immunotherapy (including nivolumab [63] and pembrolizumab [64]) has become the first-line treatment method for patients with metastatic or recurring HNSCC and the prognosis has become improved to certain degrees as a result of these interventions [65]. Although several HNSCC patients show only modest gains from immunotherapy, especially for patients with HPV-unrelated HNSCC [66,67], the overall response rate was less than 20 % [68]. In addition, immunotherapy may be rather pricey and introduces a small but real danger producing harmful side effects [69]. Therefore, personalized immunotherapy is strongly warranted and may significantly lower the incidence of adverse events. The patient's immunological landscape is what defines their individual response to immunotherapy and, ultimately, their prognosis. In this investigation, the ESTIMATE analysis for TME illustrated that low-risk patients exhibited a considerably elevated immuneScore relative to those at high risk and showed larger amounts of immune cellular components in the low-risk category. As anticipated, the proportion of T cells, including $CD4^+$ T cells, $CD8^+$ T cells, follicular helper T cells, and regulatory T cells, was higher in the low-risk samples. Proliferated and activated T cells release many cytokines and chemokines to perform a determinant function in the elimination of virally infected cells and tumor cells [70,71], which might partly explain the better outcomes observed in low-risk patients. ICB therapy is the most dominant immunotherapy in the HNSCC and works by blocking the ICGs [72] and allowing guardian T cells to identify and eliminate tumor cells [73]. Increasing evidence confirms that high ICG expression is generally correlated with improved immunotherapy efficacy [74]. We showed ICGs were overexpressed in low-risk patients. Furthermore, the IPS score of the CTLA4 blockade monotherapy, PD1 blockade monotherapy, and combination treatments with CTLA4 and PD1 blockade increased in the low-risk patients, illustrating better responsiveness to ICBs among low-risk patients. Considering the remarkable status of chemotherapy in HNSCC [75,76], we intensively explored the discrepancy in drug sensitivities between low- and high-risk patients. Chemotherapy regimens, such as cisplatin, docetaxel, gemcitabine, and paclitaxel, were shown to be more effective in high-risk patients in contrast to immunotherapy, implying that high-risk patients can derive more positive outcomes from monotherapy or combinations of chemotherapy. Overall, these findings demonstrate that our TMG signature may serve as a predictor for immunotherapy responsiveness and chemotherapy drug sensitivity. Additionally, they offer fresh insight into the individual medication choices of patients who are diagnosed with HNSCC.

Notwithstanding the positive findings obtained, this research study did have several drawbacks that ought to be considered. First, the bioinformatics analysis of public datasets is the primary method used in this particular research project. Although a validation cohort from the GEO database was included, it still requires further external validation in other cohorts with large clinical samples. Second, 12 TMGs in the signature were identified via the single-cell RNA sequencing of HNSCC. Nonetheless, the involvement of the 12 TMGs in the HNSCC and their link to T cells are still unknown and require more research. Third, there were no classic T cell markers contained in the TMG signature. Lastly, experimental verification is still lacking for both the immune features and the distinct possible mechanisms that differentiated individuals at high risk from those at lower risks.

In summary, the findings of this research study showed that T cell marker genes might be used in the single-cell RNA sequencing of HNSCC to develop a robust and independent prognostic prediction signature. Furthermore, the systematic analysis demonstrated that the risk score derived from the TMG signature was intimately linked to the prognosis, TME, immune cell infiltration status, responsiveness to immunotherapy, and chemotherapeutic sensitivity in HNSCC patients. Therefore, the TMG signature can function as an independent risk stratification and prognosis marker and provide assistance in anticipating the effectiveness of immunotherapy and chemotherapy, which will facilitate individualized clinical decisions for HNSCC patients.

4. Materials and methods

4.1. Downloading and processing data

The scRNA-seq data of 20 HNSCC samples comprising 23088 cells were derived from GSE181919 (https://www.ncbi.nlm.nih.gov/geo/query/acc.cgi?acc=GSE181919). TCGA (https://portal. gdc. cancer. gov/), containing data on 501 patients with HNSCC and 44 normal controls, was searched for bulk RNA-Seq data on gene expression as well as the respective clinical characteristics, mutations, and copy number variations (CNV) of the TCGA-HNSCC cohort. Furthermore, from the GEO database (https://www.ncbi.nlm.nih.gov/), we retrieved the GSE65858 cohort of 270 patients with HNSCC for applications as an external validation cohort. The clinical data of patients were shown in Table 1.

4.2. scRNA-seq data processing and analysis to screen the T cell marker genes

The scRNA-seq data of GSE181919 were processed with the R package "Seurat". Data were subjected to quality control to exclude low-quality cells using the following criteria: each cell has 500–4000 genes; fewer than 5 % of the genes were found in the mitochondria. Principal component analysis (PCA) and t-distributed stochastic neighbor embedding (t-SNE) techniques were applied to accomplish dimensionality reduction and cluster identification on the top 1500 high-variability genes. The "SingleR" package was applied to the cluster annotation to recognize different cell types. Subsequently, the "FindAllMarkers" function (parameters: log FC as 1 and min.pct as 0.25) was employed to identify significant marker genes for different cell types. Ultimately, TMGs were used for further analysis.

4.3. T cell marker gene-based prognostic risk model development

Differential expression and univariate Cox regression analyses, both using a $P < 0.05$ significance criterion, were applied to the TMGs discovered by scRNAseq. To identify the optimal prognostic TMGs for use in the signature's construction in the TCGA-HNSCC cohort, a LASSO regression analysis with 10-fold cross-validation was performed 1000 times by the "glmnet" package. Each HNSCC patient's risk score was determined by summing the expression levels of TMGs weighted by their coefficients from the LASSO analysis, and this was performed for both the TCGA and the GSE65858 datasets. Finally, The median risk score was established as the criterion to classify these HNSCC patients into high- and low-risk groups.

Table 1
Clinicopathological features of the head and neck squamous carcinoma patients included in this research study.

Covariates	Type	TCGA cohort		GSE65858 cohort	
		Number	Percent	Number	Percent
Age					
	≤60	246	49.10 %	130	48.15 %
	>60	255	50.90 %	140	51.85 %
Gender					
	Female	133	26.55 %	47	17.41 %
	Male	368	73.45 %	223	82.59 %
Histologic grade					
	G1-2	359	71.66 %	–	–
	G3-4	121	24.15 %	–	–
	Unknown	19	3.79 %		
T stage					
	T1-2	177	35.33 %	115	42.59 %
	T3-4	309	61.68 %	155	57.41 %
	Unknown	15	2.99 %		
N stage					
	N0	239	47.70 %	94	34.81 %
	N1-3	240	47.90 %	176	65.19 %
	Unknown	22	4.39 %		
Metastasis status					
	Yes	25	4.99 %	–	–
	No	471	94.01 %	–	–
	Unknown	5	1.00 %		
Clinical stage					
	Stage I-II	114	22.75 %	55	20.37 %
	Stage III-IV	373	74.45 %	215	79.63 %
	Unknown	14	2.79 %		
Survival status					
	Dead	217	43.31 %	94	34.81 %
	Alive	284	56.69 %	176	65.19 %

4.4. Precision and reliability of the prognostic TMG signature

To examine the differences in prognosis between high- and low-risk categories, a Kaplan–Meier (KM) survival assessment was conducted. The model's capability to anticipate 1-, 3-, and 5-year survival was evaluated by using a receiver operating characteristic (ROC) analysis. Additionally, we conducted univariate and multivariate Cox analyses to evaluate the risk score's independent predictive relevance after integrating it with clinical data. The risk model's ability to differentiate across different categories was investigated via PCA. The risk score's predictive capacity was contrasted with that of the clinical parameters using ROC curves, the C-index, and a decision curve analysis (DCA) curve. Progression-free survival (PFS) and disease-specific survival (DSS) were also evaluated as endpoints to determine the prognostic significance of the TME signature in HNSCC patients. The association between the risk score and clinical factors was assessed by using the chi-squared test and Wilcoxon rank-sum test. Moreover, to anticipate the 1-, 3-, and 5-year overall survival (OS) rate of HNSCC patients, we incorporated the risk score and clinical factors (stage, grade, sex, and age) to develop a nomogram. The predictive performance of the nomogram was calculated by utilizing the ROC, DCA, and calibration curves.

4.5. Function and gene set enrichment analysis

Low- and high-risk patients were compared using the "limma" program to identify the differentially expressed genes (DEGs) ($|\log_2 FC| > 1$ and FDR $q < 0.05$). Enrichment analyses concerning Gene Ontology (GO) and Kyoto Encyclopedia of Genes and Genomes (KEGG) pathway were carried out using DEG. Gene set enrichment analysis (GSEA) was undertaken with the aid of the GSEA software (version 4.1.0) and the reference c2.cp.kegg.v2022.1.Hs.symbols.gmt to make a comparison between high- and low-risk categories. Moreover, a Gene Set Variation Analysis (GSVA) was implemented with the "GSVA" package.

4.6. Tumor microenvironment (TME) and immune cell infiltration analysis

With the use of the ESTIMATE method, we computed the stromal, immune, and ESTIMATE scores of TME for each sample [77]. The immune and stromal scores were computed to characterize the proportion of immune cells and stromal cells that infiltrated the tumor. Non-tumor composites were reflected using ESTIMATE scores. The "GSVA" package was employed to compute a single-sample GSEA (ssGSEA) score for 13 distinct immune-associated functions. The CIBERSORT technique was applied to quantify the infiltration degree of several immune cells in the HNSCC samples [78].

4.7. Immunotherapy response and medication sensitivity prediction

The immunophenoscore (IPS) of the Cancer Immunome Database (TCIA) was employed to estimate the responsiveness to immune checkpoint blockade (ICB) (anti-CTLA-4 and anti-PD-1 immunotherapy) [79,80]. Additionally, the association of the risk score with immune checkpoint genes (ICGs), including *IDO1*, *PD1*, *PDL1*, *CTLA4*, *LAG3*, *HAVCR2*, *CD8A*, *GZMA*, *GZMB*, *PRF1*, *IFNG*, *TBX2,* and *TNF*, was explored. The "pRRophetic" R program was implemented to calculate the half-maximal inhibitory concentration (IC50) of four chemotherapeutic regimens that are often used for treating HNSCC (paclitaxel, gemcitabine, docetaxel, and cisplatin).

4.8. Analysis of the tumor mutation burden (TMB)

We employed the "maftools" R package to evaluate the somatic mutations derived from the TCGA-HNSC cohort to investigate the possible link between the risk score and TMB. The waterfall plot of the mutational landscape in both high- and low-risk categories was generated using the "GenVisR" package. The association of TMB with patient survival was evaluated by KM survival analyses.

4.9. Statistical analysis

The analyses and visualization of all statistical data were performed using the R Software (version 4.0.1). $P < 0.05$ indicated a significance level.

Funding statement

This work was funded by National Natural Science Foundation of China (No.81670920); Ningbo Technology Innovation 2025 Major Special Project (No. 2020Z097); Ningbo Natural Science Foundation (No.2019A610319, No. 202003N4239, and No. 2022J260); Ningbo Public Science Research Foundation (No. 2021S171 and No. 2021S170); Ningbo Medical and Health Brand Discipline (No. PPXK2018-02); Ningbo Clinical Research Center for Otolaryngology Head and Neck Disease (No. 2022L005); Ningbo training of young technical backbone (No.2021QNJSGG-ZCC); Zhejiang Province Medical and Health Science Research Foundation (No. 2020KY274, No. 2020RC107, No. 2021KY307, and No. 2022KY1086); Huili Fund (No. 2022YB010); and Zhejiang Provincial Natural Science Foundation (No. LY19H160014, No. LY20H130001, No. LQ21H130001, and No. LY23H130001).

Data availability statement

Data will be made available on request.

CRediT authorship contribution statement

Chongchang Zhou: Conceived and designed the experiments; Wrote the paper. **Hongxia Deng:** Conceived and designed the experiments; Wrote the paper. **Yi Fang:** Performed the experiments, Analyzed and interpreted the data. **Zhengyu Wei:** Performed the experiments, Analyzed and interpreted the data. **Yiming Shen:** Performed the experiments, Analyzed and interpreted the data. **Shijie Qiu:** Analyzed and interpreted the data. **Dong Ye:** Analyzed and interpreted the data. **Zhisen Shen:** Conceived and designed the experiments, Contributed reagents, materials, analysis tools or data, Wrote the paper. **Yi Shen:** Conceived and designed the experiments, Contributed reagents, materials, analysis tools or data, Wrote the paper.

Declaration of competing interest

The authors declare that they have no known competing financial interests or personal relationships that could have appeared to influence the work reported in this paper.

Acknowledgments

We thank all R programming package developers.

References

[1] R.L. Siegel, et al., Cancer statistics, 2022, CA Cancer J Clin 72 (1) (2022) 7–33.
[2] N. Vigneswaran, M.D. Williams, Epidemiologic trends in head and neck cancer and aids in diagnosis, Oral Maxillofac Surg Clin North Am 26 (2) (2014) 123–141.
[3] S. Marur, A.A. Forastiere, Head and neck squamous cell carcinoma: update on epidemiology, diagnosis, and treatment, Mayo Clin. Proc. 91 (3) (2016) 386–396.
[4] H. Sung, et al., Global cancer statistics 2020: GLOBOCAN estimates of incidence and mortality worldwide for 36 cancers in 185 countries, CA Cancer J Clin 71 (3) (2021) 209–249.
[5] J. Muzaffar, et al., Recent advances and future directions in clinical management of head and neck squamous cell carcinoma, Cancers 13 (2) (2021).
[6] J.D. Horton, et al., Immune evasion by head and neck cancer: foundations for combination therapy, Trends Cancer 5 (4) (2019) 208–232.
[7] O. Kaidar-Person, Z. Gil, S. Billan, Precision medicine in head and neck cancer, Drug Resist Updat 40 (2018) 13–16.
[8] N. Cohen, S. Fedewa, A.Y. Chen, Epidemiology and demographics of the head and neck cancer population, Oral Maxillofac Surg Clin North Am 30 (4) (2018) 381–395.
[9] E. Ferrari, et al., Salivary cytokines as biomarkers for oral squamous cell carcinoma: a systematic review, Int. J. Mol. Sci. 22 (13) (2021).
[10] V. Mishra, et al., Application of liquid biopsy as multi-functional biomarkers in head and neck cancer, Br. J. Cancer 126 (3) (2022) 361–370.
[11] S.H. Huang, B. O'Sullivan, Overview of the 8th edition TNM classification for head and neck cancer, Curr. Treat. Options Oncol. 18 (7) (2017) 40.
[12] D.K. Zanoni, S.G. Patel, J.P. Shah, Changes in the 8th edition of the American joint committee on cancer (AJCC) staging of head and neck cancer: rationale and implications, Curr. Oncol. Rep. 21 (6) (2019) 52.
[13] A. Schnell, et al., The yin and yang of co-inhibitory receptors: toward anti-tumor immunity without autoimmunity, Cell Res. 30 (4) (2020) 285–299.
[14] C. Li, et al., Regulatory T cells in tumor microenvironment: new mechanisms, potential therapeutic strategies and future prospects, Mol. Cancer 19 (1) (2020) 116.
[15] G.T. Motz, G. Coukos, Deciphering and reversing tumor immune suppression, Immunity 39 (1) (2013) 61–73.
[16] E.J. Wherry, T cell exhaustion, Nat. Immunol. 12 (6) (2011) 492–499.
[17] X. Le, et al., Evolving role of immunotherapy in recurrent metastatic head and neck cancer, J Natl Compr Canc Netw 18 (7) (2020) 899–906.
[18] X. Qi, et al., Advances in T-cell checkpoint immunotherapy for head and neck squamous cell carcinoma, OncoTargets Ther. 10 (2017) 5745–5754.
[19] W.Y. Chen, et al., Prognostic significance of tumor-infiltrating lymphocytes in patients with operable tongue cancer, Radiat. Oncol. 13 (1) (2018) 157.
[20] I. Seminerio, et al., Infiltration of FoxP3+ regulatory T cells is a strong and independent prognostic factor in head and neck squamous cell carcinoma, Cancers 11 (2) (2019).
[21] S. Shimizu, et al., Tumor-infiltrating CD8(+) T-cell density is an independent prognostic marker for oral squamous cell carcinoma, Cancer Med. 8 (1) (2019) 80–93.
[22] G.S. Kinker, et al., Pan-cancer single-cell RNA-seq identifies recurring programs of cellular heterogeneity, Nat. Genet. 52 (11) (2020) 1208–1218.
[23] A. Kulkarni, et al., Beyond bulk: a review of single cell transcriptomics methodologies and applications, Curr. Opin. Biotechnol. 58 (2019) 129–136.
[24] Z. Pan, et al., Identification and analysis of a CD8+ T cell-related prognostic signature for colorectal cancer based on bulk RNA sequencing and scRNA sequencing data: a STROBE-compliant retrospective study, Medicine (Baltim.) 101 (39) (2022), e30758.
[25] X. Yu, et al., Single-cell sequencing and establishment of an 8-gene prognostic model for pancreatic cancer patients, Front. Oncol. 12 (2022), 1000447.
[26] J.D. Cramer, et al., The changing therapeutic landscape of head and neck cancer, Nat. Rev. Clin. Oncol. 16 (11) (2019) 669–683.
[27] M. Amoils, et al., Node-positive cutaneous squamous cell carcinoma of the head and neck: survival, high-risk features, and adjuvant chemoradiotherapy outcomes, Head Neck 39 (5) (2017) 881–885.
[28] C.A. Karvonen-Gutierrez, et al., Quality of life scores predict survival among patients with head and neck cancer, J. Clin. Oncol. 26 (16) (2008) 2754–2760.
[29] G.V. Sharonov, et al., B cells, plasma cells and antibody repertoires in the tumour microenvironment, Nat. Rev. Immunol. 20 (5) (2020) 294–307.
[30] R. Basu, et al., Cytotoxic T cells use mechanical force to potentiate target cell killing, Cell 165 (1) (2016) 100–110.
[31] J. Fang, et al., Prognostic significance of tumor infiltrating immune cells in oral squamous cell carcinoma, BMC Cancer 17 (1) (2017) 375.
[32] N. Nguyen, et al., Tumor infiltrating lymphocytes and survival in patients with head and neck squamous cell carcinoma, Head Neck 38 (7) (2016) 1074–1084.
[33] L. Chen, et al., Comprehensive analyses of a CD8(+) T cell infiltration related gene signature with regard to the prediction of prognosis and immunotherapy response in lung squamous cell carcinoma, BMC Bioinf. 24 (1) (2023) 238.
[34] T. Kuang, et al., Construction of a T-cell exhaustion-related gene signature for predicting prognosis and immune response in hepatocellular carcinoma, Aging (Albany NY) 15 (12) (2023) 5751–5774.
[35] X. Liu, et al., Tumor microenvironment CD8 T and treg cells-related genes signature distinguishes distinct prognosis and targeted therapies response in endometrial cancer, J. Immunother. 46 (5) (2023) 178–191.

[36] A.E. Oja, et al., GITR shapes humoral immunity by controlling the balance between follicular T helper cells and regulatory T follicular cells, Immunol. Lett. 222 (2020) 73–79.
[37] A.A. van Beek, et al., GITR ligation enhances functionality of tumor-infiltrating T cells in hepatocellular carcinoma, Int. J. Cancer 145 (4) (2019) 1111–1124.
[38] M.A. Gamaleldin, S.A.E. Imbaby, The role of tumor necrosis factor receptor superfamily member 4 (TNFRSF4) gene expression in diagnosis and prognosis of acute myeloid leukemia, Mol. Biol. Rep. 48 (10) (2021) 6831–6843.
[39] M. Marconato, et al., Expression of the immune checkpoint modulator OX40 indicates poor survival in acute myeloid leukemia, Sci. Rep. 12 (1) (2022), 15856.
[40] R. Sawada, et al., High blood levels of soluble OX40 (CD134), an immune costimulatory molecule, indicate reduced survival in patients with advanced colorectal cancer, Oncol. Rep. 42 (5) (2019) 2057–2064.
[41] K. Hayashi, N. Anzai, L-type amino acid transporter 1 as a target for inflammatory disease and cancer immunotherapy, J. Pharmacol. Sci. 148 (1) (2022) 31–40.
[42] K. Sato, et al., Significant relationship between the LAT1 expression pattern and chemoresistance in ovarian clear cell carcinoma, Virchows Arch. 474 (6) (2019) 701–710.
[43] B.W. Liao, et al., FAM177A1 inhibits IL-1beta-induced signaling by impairing TRAF6-ubc13 association, J. Immunol. 207 (12) (2021) 3090–3097.
[44] Y. Chen, et al., LIMD2 is a prognostic and predictive marker in patients with esophageal cancer based on a ceRNA network analysis, Front. Genet. 12 (2021), 774432.
[45] Q.Y. Zhong, et al., LIMD2 promotes tumor proliferation, invasion, and epithelial-mesenchymal transition in clear cell renal cell carcinoma, Neoplasma 69 (4) (2022) 832–840.
[46] L. Chen, et al., LIM domain-containing 2 (LIMD2) promotes the progress of ovarian cancer via the focal adhesion signaling pathway, Bioengineered 12 (2) (2021) 10089–10100.
[47] R.P. Araldi, et al., LIMD2 regulates key steps of metastasis cascade in papillary thyroid cancer cells via MAPK crosstalk, Cells 9 (11) (2020).
[48] E. Widegren, et al., Expression of FXYD3 protein in relation to biological and clinicopathological variables in colorectal cancers, Chemotherapy 55 (6) (2009) 407–413.
[49] S. Yonekura, K. Ueda, FXYD3 expression predicts poor prognosis in renal cell carcinoma with immunosuppressive tumor microenvironment, Cancers 14 (15) (2022).
[50] D. Shiba, et al., Clinicopathological significance of cystatin A expression in progression of esophageal squamous cell carcinoma, Medicine (Baltim.) 97 (15) (2018) e0357.
[51] Y. Wang, et al., Decreased CSTA expression promotes lymphatic metastasis and predicts poor survival in oral squamous cell carcinoma, Arch. Oral Biol. 126 (2021), 105116.
[52] K. Kostov, A. Blazhev, Changes in serum levels of matrix metalloproteinase-1 and tissue inhibitor of metalloproteinases-1 in patients with essential hypertension, Bioengineering (Basel) 9 (3) (2022).
[53] Y. Tan, et al., TIMP1 down-regulation enhances gemcitabine sensitivity and reverses chemoresistance in pancreatic cancer, Biochem. Pharmacol. 189 (2021), 114085.
[54] J. Muri, M. Kopf, Redox regulation of immunometabolism, Nat. Rev. Immunol. 21 (6) (2021) 363–381.
[55] F. Lu, et al., Thioredoxin 1 supports colorectal cancer cell survival and promotes migration and invasion under glucose deprivation through interaction with G6PD, Int. J. Biol. Sci. 18 (14) (2022) 5539–5553.
[56] S. Ribback, et al., Thioredoxin 1 (Trx1) is associated with poor prognosis in clear cell renal cell carcinoma (ccRCC): an example for the crucial role of redox signaling in ccRCC, World J. Urol. 40 (3) (2022) 739–746.
[57] M. Di Sanzo, et al., Ferritin heavy chain binds peroxiredoxin 6 and inhibits cell proliferation and migration, Int. J. Mol. Sci. 23 (21) (2022).
[58] B.M. Gumbiner, Cell adhesion: the molecular basis of tissue architecture and morphogenesis, Cell 84 (3) (1996) 345–357.
[59] J.S. Hale, M. Li, J.D. Lathia, The malignant social network: cell-cell adhesion and communication in cancer stem cells, Cell Adh Migr 6 (4) (2012) 346–355.
[60] A. Ali, et al., Characterization of the rainbow trout spleen transcriptome and identification of immune-related genes, Front. Genet. 5 (2014) 348.
[61] M. Huse, The T-cell-receptor signaling network, J. Cell Sci. 122 (Pt 9) (2009) 1269–1273.
[62] I. Lasinska, et al., Immunotherapy in patients with recurrent and metastatic squamous cell carcinoma of the head and neck, Anti Cancer Agents Med. Chem. 19 (3) (2019) 290–303.
[63] R.L. Ferris, et al., Nivolumab for recurrent squamous-cell carcinoma of the head and neck, N. Engl. J. Med. 375 (19) (2016) 1856–1867.
[64] R. Mehra, et al., Efficacy and safety of pembrolizumab in recurrent/metastatic head and neck squamous cell carcinoma: pooled analyses after long-term follow-up in KEYNOTE-012, Br. J. Cancer 119 (2) (2018) 153–159.
[65] H. Shaikh, V. Karivedu, T.M. Wise-Draper, Managing recurrent metastatic head and neck cancer, Hematol. Oncol. Clin. N. Am. 35 (5) (2021) 1009–1020.
[66] R.B. Bell, et al., Moving beyond the T cell synapse for combination neoadjuvant immunotherapy in head and neck cancer, J. Clin. Invest. 132 (18) (2022).
[67] S. Trivedi, L. Sun, C. Aggarwal, Immunotherapy for head and neck cancer, Hematol. Oncol. Clin. N. Am. 35 (5) (2021) 1021–1037.
[68] T.Y. Seiwert, et al., Safety and clinical activity of pembrolizumab for treatment of recurrent or metastatic squamous cell carcinoma of the head and neck (KEYNOTE-012): an open-label, multicentre, phase 1b trial, Lancet Oncol. 17 (7) (2016) 956–965.
[69] N. Choudhury, Y. Nakamura, Importance of immunopharmacogenomics in cancer treatment: patient selection and monitoring for immune checkpoint antibodies, Cancer Sci. 107 (2) (2016) 107–115.
[70] S. Li, et al., Prolonged activation of innate immune pathways by a polyvalent STING agonist, Nat. Biomed. Eng. 5 (5) (2021) 455–466.
[71] J. Pramanik, et al., Genome-wide analyses reveal the IRE1a-XBP1 pathway promotes T helper cell differentiation by resolving secretory stress and accelerating proliferation, Genome Med. 10 (1) (2018) 76.
[72] D.M. Pardoll, The blockade of immune checkpoints in cancer immunotherapy, Nat. Rev. Cancer 12 (4) (2012) 252–264.
[73] J.D. Cramer, B. Burtness, R.L. Ferris, Immunotherapy for head and neck cancer: recent advances and future directions, Oral Oncol. 99 (2019), 104460.
[74] N. Gavrielatou, et al., Biomarkers for immunotherapy response in head and neck cancer, Cancer Treat Rev. 84 (2020), 101977.
[75] S.A. Bhide, C.M. Nutting, Advances in chemotherapy for head and neck cancer, Oral Oncol. 46 (6) (2010) 436–438.
[76] A. Rajendra, et al., Palliative chemotherapy in head and neck cancer: balancing between beneficial and adverse effects, Expert Rev. Anticancer Ther. 20 (1) (2020) 17–29.
[77] K. Yoshihara, et al., Inferring tumour purity and stromal and immune cell admixture from expression data, Nat. Commun. 4 (2013) 2612.
[78] A.M. Newman, et al., Robust enumeration of cell subsets from tissue expression profiles, Nat. Methods 12 (5) (2015) 453–457.
[79] W. Hugo, et al., Genomic and transcriptomic features of response to anti-PD-1 therapy in metastatic melanoma, Cell 165 (1) (2016) 35–44.
[80] E.M. Van Allen, et al., Genomic correlates of response to CTLA-4 blockade in metastatic melanoma, Science 350 (6257) (2015) 207–211.